Geophys. J. Int. (2004) **157,** 25–35 doi: 10.1111/j.1365-246X.2004.02208.x

Consistent atmospheric and oceanic excitation of the Earth's free polar motion

Florian Seitz,[1] Jochen Stuck[2] and Maik Thomas[3]

[1] *Deutsches Geodätisches Forschungsinstitut, Marstallplatz* 8*, München* D-80539, *Germany. E-mail: florian.seitz@dgfi.badw.de*
[2] *Meteorologisches Institut, Universität Bonn, Auf dem Hügel* 20*, Bonn* D-53121, *Germany. E-mail: j.stuck@uni-bonn.de*
[3] *Institut für Planetare Geodäsie, Technische Universität Dresden, Mommsenstrasse 13, Dresden* D-01062, *Germany. E-mail: mthom@rcs.urz.tu-dresden.de*

Accepted 2003 November 24. Received 2003 October 31; in original form 2003 May 9

SUMMARY

Earth orientation parameters as observed by space-geodetic techniques show a broad spectrum of frequencies. Many efforts have been made to relate spectral peaks to geophysical processes, such as atmospheric or oceanic variations. However, the mechanisms of excitation of some typical oscillations are still unclear. In order to gain insight into the rotational dynamics of the Earth, the non-linear gyroscopic Dynamic Model for Earth Rotation and Gravity (DyMEG) has been developed at DGFI (Deutsches Geodätisches Forschungsinstitut). The present paper studies the superposed effect of atmospheric and oceanic excitation on the free rotation of a viscoelastic gyro. In contrast to former investigations, period and damping of the Earth's free wobble (Chandler wobble) are generated by the gyro from geometrical and rheological parameters. Numerical results for polar motion in the time domain demonstrate that DyMEG creates a damped oscillation in absence of geophysical and gravitational excitations. Damping vanishes when atmospheric and oceanic angular momentum is regarded. Simulated polar motion for the period from 1975 to 1994 forced by consistent atmospheric and oceanic angular momentum shows significant correlation with geodetic observations, which indicates that the free gyroscopic model DyMEG is able to reproduce realistic variations of the Earth's rotation. Spectral analyses of both atmospheric and oceanic excitations give no hint for increased power in the Chandler frequency band as it was stated for the maintenance of the Chandler wobble in recent research studies. Thus, stochastic signals in the climate dynamics as caused by both the weather and oceanic mass redistributions are found to be a sufficient source to maintain the amplitude of the Earth's free wobble by resonant interaction.

Key words: atmosphere, Earth's rotation, oceans, polar motion, wobble.

1 INTRODUCTION

Mass redistributions outside or inside the Earth caused by geophysical processes and gravitational interactions with celestial bodies influence the rotational dynamics of the Earth on subdaily to secular timescales. They are reflected by polar motion, changes in length-of-day (ΔLOD) and modifications of the amplitudes and phases of the nutation components for a rigid Earth. The variations of Earth's rotation as a result of these excitations are additionally superposed by free oscillations of the Earth, i.e. the Chandler wobble and the nearly diurnal free wobble.

For the last few decades, space-geodetic techniques have provided time-series of Earth's rotation parameters with increasing accuracy (IERS 2003). The results of the observations represent the integral effects of redistributions and motions of masses in the Earth's fluid components, however, they do not allow for conclusions with respect to their individual causative processes. Hence, independent approaches from theory and modelling are needed for understanding both the geophysically-induced global mass transports and the dynamic response of the Earth.

To gain insight into the rotational dynamics of the Earth, the non-linear gyroscopic Dynamic Model for Earth Rotation and Gravity (DyMEG) has been developed (Seitz & Kutterer 2002). The characteristics of the Earth's free polar motion are generated by the model based on rheological and geometrical parameters. Thus, the gyro is alternative to previous studies (Lambeck 1980) as the numerical model dispenses with any explicit information concerning amplitude, phase and period of the free oscillations.

It is well known that the amplitude of the Chandler wobble would diminish as a result of frictional effects without further excitation (Moritz & Mueller 1987). However, time-series derived from geodetic observations do not show any damping. The reason for the perpetuation of the Chandler amplitude is still not well understood and was, so far, looked for in solitary components of the Earth system. It

was assumed that either atmospheric or hydrologic mass redistributions (Wahr 1983; Hameed & Currie 1989; Sidorenkov 1992; Furuya *et al.* 1996, 1997), or processes in the Earth's interior (Souriau & Cazenave 1985; Gross 1986; Hinderer *et al.* 1987) are responsible for the excitation of the Chandler wobble. Recently, Gross (2000) concluded from a spectral analysis of atmospheric wind and pressure data from the NCEP/NCAR reanalysis project, and currents and bottom pressure fields of the global ocean general circulation model of the Massachusetts Institute of Technology (MIT), that, in particular, the excitation power resulting from oceanic bottom pressure variations in a Chandler frequency band between 0.730 cpy and 0.913 cpy is sufficient to excite the Chandler wobble during 1985–1996.

Different to Gross (2000) whose investigation was performed in the frequency domain, this study compares the resulting polar motion series with geodetic observations in the time domain. In the following, it is shown that the damped free oscillation, which is produced by the gyroscopic model of Seitz & Kutterer (2002) in absence of geophysical excitations, is perpetuated when the combined effects of consistent simulated atmospheric and oceanic excitation are taken into account, although no increased excitation power can be found in the Chandler band of the respective excitations.

2 CONFIGURATION AND PROPERTIES OF THE GYROSCOPIC MODEL DyMEG

2.1 Liouville differential equation

The gyroscopic model is based on the balance of angular momentum. In a terrestrial reference system, the Earth's reaction on mass redistributions can be described by the Liouville differential equation (Munk & MacDonald 1960):

$$\frac{d}{dt}\left(\underline{\boldsymbol{I}}\boldsymbol{\omega}+\mathbf{h}\right)+\boldsymbol{\omega}\times\left(\underline{\boldsymbol{I}}\boldsymbol{\omega}+\mathbf{h}\right)=\mathbf{L}, \tag{1}$$

where $\underline{\boldsymbol{I}}$ denotes the Earth's tensor of inertia, the vectors $\mathbf{h}$ and $\mathbf{L}$ denote angular momentum with respect to the reference system and torques resulting from gravitational forces of the Sun and Moon, respectively, and $\boldsymbol{\omega}$ is the rotation vector of the terrestrial system with respect to an inertial system.

Variations of Earth's rotation are interpreted as small deviations from a uniform rotation. The z-axis of the terrestrial reference system is oriented approximately towards the Earth's maximum moment of inertia C and the equatorial axes x and y point towards the Greenwich meridian and 90°E, respectively. In this system, the coordinates of the rotation vector $\boldsymbol{\omega}$ are expressed by

$$\boldsymbol{\omega}=\Omega\cdot\begin{pmatrix} m_1 \\ m_2 \\ 1+m_3 \end{pmatrix}, \tag{2}$$

where $\Omega = 2\pi/86164$ s denotes the approximate angular velocity of the terrestrial system. The dimensionless quantities $m_i (i = 1, 2, 3)$ represent slight disturbances of the uniform rotation and arise as unknown parameters in the Liouville differential equation (Munk & MacDonald 1960). The two components m_1 and m_2 describe the orientation of the instantaneous rotation axis with respect to the z-axis of the inertial system (polar motion). Deviations of the Earth's angular velocity with respect to Ω, which are equivalent to changes of the length-of-day (ΔLOD), follow from the temporal variation of the absolute value of the Earth's rotation vector $|\boldsymbol{\omega}| \approx \Omega\,(1+m_3)$. The error for ΔLOD resulting from this approximation is 10^{-16} s and therefore negligible.

Mass redistributions in the Earth's fluid components, e.g. in the atmosphere and the oceans, cause perturbations of the tensor of inertia and relative angular momentum. Thus, all quantities in the Liouville equation are time-dependent. Numerical values of these quantities are provided by atmospheric and oceanic model simulations (*cf*. Section 4.1). The tensor of inertia is additionally influenced by deformations of the Earth's body as a result of loading, solid Earth tides and rotational variations.

Provided that the tensor of inertia $\underline{\boldsymbol{I}}(t)$, relative angular momentum $\mathbf{h}(t)$ and torques $\mathbf{L}(t)$ can be calculated with sufficient precision for each time step, variations of Earth's rotation result from solving the Liouville equation for $\boldsymbol{\omega}(t)$.

2.2 Analytical approach

Traditionally, the Liouville equation is solved by introducing a couple of simplifications. The equatorial principal moments of inertia A and B are set equal, i.e. the ellipsoid of inertia on which the calculation is based is assumed to be rotationally symmetric and eq. (1) is linearized. Hence, the horizontal components of the Earth's rotation vector are decoupled from the axial component (Munk & MacDonald 1960). Thus, the linearized Liouville differential equation can be written as

$$\begin{aligned} m_1 - \dot{m}_2/\sigma_0 &= \Psi_1 \\ m_2 + \dot{m}_1/\sigma_0 &= \Psi_2 \\ \dot{m}_3 &= \dot{\Psi}_3, \end{aligned} \tag{3}$$

where the so-called excitation functions $\Psi_i (i = 1, 2, 3)$ comprehend variations in the tensor of inertia $\Delta\underline{\boldsymbol{I}}(t)$ and relative angular momentum $\mathbf{h}(t)$, which are the result of geophysically- and gravitationally-induced mass redistributions and the lunisolar torques $\mathbf{L}(t)$ (Wahr 1982). The Chandler frequency σ_0 is pre-selected in this linearized approach and has a constant value (Lambeck 1980).

Adopting these simplifications enables an analytical solution of the equations for polar motion by transforming them into complex notation. The resulting values for $m(t) = m_1(t) + i m_2(t)$ due to the excitation $\Psi(t) = \Psi_1(t) + i\Psi_2(t)$ are derived from

$$m(t) = e^{i\sigma_0(t-t_0)}\left[m_0 - i\sigma_0\int_{t_0}^{t}\Psi(\tau)e^{-i\sigma_0\tau}\,d\tau\right], \tag{4}$$

where m_0 denotes the initial value at time $t = t_0$. Results for ΔLOD are obtained independently from the axial component of the Liouville equation (Munk & MacDonald 1960).

However, as the frequency of the Earth's free oscillation is introduced into the linearized model using the fixed value σ_0, the analytical approach is not capable of accounting for the interactions between geophysical and gravitational forcing and the Earth's free wobble, which are expected from rotational deformations. It is well known, that the prolongation of the Euler period of 304 d, which is the period of the free wobble of a rigid Earth, to the observed Chandler period of approximately 432 d is the result of rotational deformations of the Earth's body (Moritz & Mueller 1987). Changes in the centrifugal potential, which are caused by mass redistributions, yield back-coupling effects on the tensor of inertia. Consequently, time-varying mass distributions are accompanied by modified resonance conditions of the Earth. Therefore, both amplitude and frequency of the Chandler wobble are time variable as they are directly influenced by the excitations.

2.3 Numerical approach

To overcome the deficiencies of the linearized approach, a numerical model has been developed. No explicit information about the

Chandler frequency σ_0 shall be predetermined in DyMEG. Hence, σ_0 is not a degree of freedom and the Earth's free polar motion has to be produced from the gyroscopic model based on rheological and geometrical parameters. As the effects of rotational deformations are regarded, DyMEG is able to react on rotational variations. Consequently the model is suitable for studies of the interaction between forced and free polar motion. In order to achieve the aim of a completely free gyro, the traditional analytical procedure cannot be applied as the prerequisite for the analytical solution is the introduction of the Chandler frequency σ_0 into eq. (4). Hence, the Liouville differential equation has to be evaluated numerically. Eq. (1) is rewritten as a coupled system of three first-order differential equations that can be solved as an initial value problem:

$$\begin{pmatrix} \dot{m}_1 \\ \dot{m}_2 \\ \dot{m}_3 \end{pmatrix} = \frac{1}{\Omega} \underline{\boldsymbol{I}}^{-1} \left(\mathbf{L} - \dot{\underline{\boldsymbol{I}}}\boldsymbol{\omega} - \dot{\mathbf{h}} - \boldsymbol{\omega} \times \mathbf{h} - \boldsymbol{\omega} \times \underline{\boldsymbol{I}}\boldsymbol{\omega} \right) \tag{5}$$

Initial values for $m_i(t = t_0)$ are deduced from the geodetically observed time-series for polar motion and length-of-day variations, which are published in the C04 series by the International Earth Rotation Service (IERS 2003). The values $m_i(t = t_0)$ are related to observations and their respective time derivatives at $t = t_0$ (Gross 1992). Supplementary conditions for subsequent dates $m_i(t \neq t_0)$ are not provided in order to obtain numerical results that are unconstrained with respect to observations (free model). In contrast to the traditional analytical approach, polar motion and ΔLOD are computed simultaneously in DyMEG and linearization is not necessary. Consequently, temporal variations of all elements of the full tensor of inertia can be considered and the products of the small quantities $\Delta \boldsymbol{I}_{ij}$ $(i, j = 1, 2, 3)$, $\mathbf{h}_i$ and m_i, which are commonly neglected, are contained in the solution, too.

The sensitivity of the numerical solution with respect to the choice of the initial values $m_i(t = t_0)$ was tested by varying the values within the interval $\pm 3\sigma_i$ with respect to the observations of polar motion and ΔLOD, which have the standard deviations σ_i. As the initial amplitude of the Chandler wobble and its phase are directly linked to $m_1(t = t_0)$ and $m_2(t = t_0)$, DyMEG was expected to be rather sensitive to variations of the initial values. However, the sensitivity analysis revealed that the interpretation of the numerical results is not limited by the choice of the initial values as long as the values stay within these reasonable intervals (Seitz & Kutterer 2004).

As a side-effect, the numerical solution of the system enables the use of differing values for the equatorial principal moments of inertia A and B. From the analyses of new satellite missions, the values of A, B and C can be determined with high accuracy as well as the directions of the principal axes of inertia with respect to the rotating reference system (Marchenko & Schwintzer 2003). Although the difference between A and B is marginal, the assumption of a rotationally symmetric ellipsoid of inertia leads to a non-negligible effect on the polar motion time-series as the period of the free wobble is shortened approximately 2 d when recent estimates of both the principal moments of inertia and rheological parameters are introduced into DyMEG (*cf*. Section 3). Consequently, as a result of this frequency shift two polar motion results for which the same geometrical and rheological parameters are applied diverge gradually when they are based on a biaxial and triaxial ellipsoid of inertia, respectively. Conversely, in order to obtain the same frequency for the Earth's free polar motion using a simplified biaxial, instead of a triaxial, ellipsoid of inertia, the rheological parameters, i.e. the Love numbers, have to be adapted (Seitz & Kutterer 2004). As the accuracy of the free polar motion period is limited as a result of the biaxial simplification, the above study reveals a deficiency of the analytical solution. When a triaxial and a biaxial model is run with adapted Love numbers, so that the free oscillations of both time-series feature a concordant period, the remaining difference of the polar motion amplitude is up to ± 7 mas. Hence, the model error resulting from the simplification exceeds the accuracy of modern space-geodetic observations even though it is small compared with the present accuracy of modelling.

Time-series of the tensor of inertia are calculated by superposing the effects of rotational deformations, solid Earth tides (McCarthy 2003) and excitations resulting from mass redistributions in the fluid Earth components atmosphere and oceans. The latter are calculated from consistent model simulations. Relative angular momentum $\mathbf{h}(t)$, which is mainly caused by oceanic and atmospheric currents, is additionally provided from those model simulations and the gravitational torques $\mathbf{L}(t)$ are calculated from lunisolar ephemeris (Munk & MacDonald 1960). Besides this, the indirect effect on the Earth's tensor of inertia resulting from loading deformation is calculated via Green's functions from the simulated atmospheric surface and oceanic bottom pressure variations (Moritz & Mueller 1987). For the numerical evaluation of eq. (5), a one-step-solver based on the fourth/fifth-order Runge–Kutta–Fehlberg method is applied (Press *et al.* 1987).

3 FREE WOBBLE OF THE GYROSCOPIC MODEL

To study the free oscillations of the gyro, and consequently the reliability of underlying numerical parameters, any geophysical and gravitational excitations and external torques are neglected in a first step, i.e. only the effect of rotational deformations is regarded. Temporal variations of the rotation vector $\boldsymbol{\omega}(t)$ lead to variations of the centrifugal potential and thus yield deformations of the Earth's body. While the deformations resulting from ΔLOD are far below mm level and are therefore negligible, deformations resulting from polar motion produce significant effects on the Earth's rotational dynamics (Wahr 1985).

The back-coupling effects of rotational deformations are described by disturbances of the geopotential coefficients $\Delta C_{21}(t)$ and $\Delta S_{21}(t)$. As variations of the second-order potential coefficients are directly linked to the elements of $\Delta \underline{\mathbf{I}}(t)$ (Lambeck 1980), the resulting time-series for $\Delta C_{21}(t)$ and $\Delta S_{21}(t)$ are transformed into perturbations of the tensor of inertia and thus introduced into the model. For investigations of Earth's rotation, contributions of higher-degree spherical harmonic coefficients are negligible (McCarthy 2003):

$$\begin{aligned} \Delta C_{21} &= -\frac{\Omega^2 a^3}{3GM} \left(\Re k_2 \cdot m_1 + \Im k_2 \cdot m_2 \right) + \mathcal{O}^2 \\ \Delta S_{21} &= -\frac{\Omega^2 a^3}{3GM} \left(\Re k_2 \cdot m_2 - \Im k_2 \cdot m_1 \right) + \mathcal{O}^2, \end{aligned} \tag{6}$$

where a denotes the Earth's mean equatorial radius, G is the gravitational constant and M is the total mass of the Earth. The effects on the centrifugal potential resulting from the rheological characteristics of the model body are described by the complex pole tide Love number $k_2 = \Re k_2 + i \cdot \Im k_2$. Second-order terms $\mathcal{O}^2$ are neglected.

The model simulations start at 1962 January 1, i.e. the beginning of the time-series C04 from which initial values for m_i are determined. The triaxial tensor of inertia $\underline{\boldsymbol{I}}_0$, which represents the approximate tensor of inertia of the Earth, is introduced into the Liouville equation (eq. 1). Neither gravitational nor atmospheric

and oceanic excitations are included in this experiment. Thus, there are no contributions to the tensor of inertia except the rotational deformations. Furthermore $\mathbf{h}(t)$ and $\mathbf{L}(t)$ equal zero.

Numerical solution of the differential eq. (5) allows a calculation of the potential coefficients from the results for $m_i(t)$ according to eq. (6). The obtained perturbation moments $\Delta\underline{\boldsymbol{I}}(t)$ describe the mass redistributions caused by rotational deformations. They are subsequently superposed to the tensor $\underline{\boldsymbol{I}}_0$ of the ellipsoid of inertia and are used for the computation at the next time step.

When the (preliminary) value $k_2^* = 0.30088$ is introduced for the pole tide Love number, DyMEG produces a free oscillation with a period of 447 d. Both values are in concordance with Smith & Dahlen (1981) who illustrate that this period is appropriate for a purely elastic Earth neglecting the dynamic response of core and oceans. This first result demonstrates that numerical time-series derived from the gyroscopic model agree with theory. The initial tensor of inertia $\underline{\boldsymbol{I}}_0$ that is applied in this experiment has the form

$$\underline{\boldsymbol{I}}_0 = \begin{pmatrix} A & 0 & 0 \\ 0 & B & 0 \\ 0 & 0 & C \end{pmatrix}, \tag{7}$$

where A, B and C denote the Earth's principal moments of inertia. The discrepancy between the principal axes of inertia and the axes of the reference system is taken into account by means of a rotation (Marchenko & Schwintzer 2003).

In order to refine the Earth's reaction on rotational variations, the effects of the dynamic fluid core, the equilibrium ocean pole tides and the mantle anelasticity have to be taken into account for the computation of rotational deformations (Smith & Dahlen 1981). In the following, a simple Earth model is employed that consists of an anelastic mantle and a spherical liquid core, which are assumed to be completely decoupled. Basic considerations about the application of such a model body for studies on Earth's rotation can be found in, for example, Moritz & Mueller (1987) and Brzezinski (2001). They are similar to the models introduced by Molodensky (1961) and Sasao *et al.* (1980), however, in contrast to these latter studies, DyMEG does not account for angular momentum exchanges between core and mantle. Here, further improvement of the model is necessary, although the effects of core–mantle coupling on polar motion are significant mainly on subdaily timescales. However, huge decadal variations of ΔLOD are caused by core–mantle interaction. To account for their influence on the Earth's angular velocity, direct time-series of length-of-day changes as provided by the Special Bureau for the Core of the IERS Global Geophysical Fluids Center (GGFC) are considered (Ponsar *et al.* 2002).

As a consequence of the decoupling of core and mantle, the principal moments of inertia A, B and C, which are introduced into the initial tensor of inertia $\underline{\boldsymbol{I}}_0$, have to be replaced by A_m, B_m and C_m, which are attributed to the mantle alone. As the core is assumed to be spherical, the principal moments of inertia used for the computation are derived from $A_m = A - A_c$, $B_m = B - A_c$ and $C_m = C - A_c$. Here, A_c denotes the principal moment of inertia of a spherical core. Its value is derived from

$$A_c = A\frac{\xi}{\gamma} \tag{8}$$

(Sasao *et al.* 1980), where ξ and γ are constants that depend on the rheological properties of mantle and core. The values given in Sasao *et al.* (1980) are $\xi = 2.300 \times 10^{-4}$ and $\gamma = 1.970 \times 10^{-3}$. In a more recent study, Mathews *et al.* (1991) computed $\xi = 2.222 \times 10^{-4}$ and $\gamma = 1.965 \times 10^{-3}$ from the Earth Model PREM (Dziewonski & Anderson 1981).

Surcharges to the above given value for the elastic pole tide Love number k_2^* have to be added in order to account for the effects of ocean pole tides and mantle anelasticity. The effective pole tide Love number k_2 can be written as

$$k_2 = k_2^* + \Delta k_2^O + \Delta k_2^A, \tag{9}$$

where Δk_2^O and Δk_2^A denote the incremental corrections due to the ocean pole tides and the anelastic response, respectively. In recent research studies, appropriate supplements to the Love number k_2^* were determined. Referring to Mathews *et al.* (2002) and Smith & Dahlen (1981), the contribution of the equilibrium ocean pole tides amounts to approximately $\Delta k_2^O = 0.044$.

As the reaction of the Earth's mantle on variations of the geopotential is not purely elastic, a time lag between the variation of the rotation vector $\boldsymbol{\omega}$ and the deformations of the mantle emerges. Furthermore, this anelastic response is accompanied by energy dissipation, which leads to an attenuation of the free wobble. In the model, the mantle anelasticity is considered by adding the complex supplement $\Delta k_2^A = 0.0125 + 0.0035i$ to the Love number k_2^* (McCarthy 2003; Mathews *et al.* 2002). As a consequence, the free oscillation of the gyro is a damped oscillation that would diminish if no excitation mechanism would counteract the dissipation (Moritz & Mueller 1987).

Summing up the above mentioned effects of oceans, core and mantle, the value of the final pole tide Love number to be introduced into DyMEG is $k_2 = 0.35 + 0.0035i$. Substitution of k_2^* by k_2 yields a period of 431.9 d for the free wobble of the gyroscopic model. This value coincides with the mean Chandler period derived from the C04 series by means of spectral analysis.

Fig. 1 shows the normalized model result of the x-component of polar motion covering 33 yr from 1962 January 1 through 1995 December 31. The temporal resolution of the model output amounts to 12 h. The damping of the Chandler amplitude resulting from the anelastic behaviour of the Earth's mantle is obvious. As no further excitation influences the Earth's tensor of inertia, there is no back-coupling between geophysical or gravitational processes and the free oscillation. Therefore, the Chandler frequency remains constant.

The damping function $c(t)$, which is the envelope of the damped oscillation, is given by

$$c(t) = c_0 \cdot e^{-\delta(t-t_0)}, \tag{10}$$

where c_0 is the initial amplitude of the oscillation and δ is the damping coefficient. The latter value is derived from the proportion of two subsequent maxima of the oscillation $c_i(t_i)$ and $c_{i+1}(t_{i+1})$:

$$\delta = \frac{\ln(c_i/c_{i+1})}{(t_{i+1} - t_i)}. \tag{11}$$

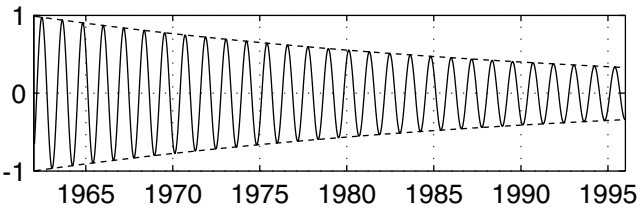

Figure 1. Damped free wobble as derived from DyMEG in absence of atmospheric and oceanic excitations and torques (normalized representation). The solid line represents the x-coordinate of the simulated polar motion regarding ocean pole tides, core decoupling and mantle anelasticity. The dashed line shows the damping function.

In general, the damping resulting from rotational deformations is expressed in terms of a quality factor Q. The reciprocal value Q^{-1} represents the specific dissipation, which provides information about the energy dissipation in the Earth at the Chandler frequency (Munk & MacDonald 1960). The specific dissipation can directly be deduced from the damping coefficient:

$$Q^{-1} = \frac{\delta\,(t_{i+1} - t_i)}{\pi}. \tag{12}$$

Fitting the function eq. (10) to the model result (Fig. 1) yields a quality factor of $Q = 84$. A critical discussion of this value will be given below.

When geophysical and gravitational forcing is introduced into the gyroscopic model, an effect on the Chandler wobble is expected as a consequence of modified resonance conditions. As the temporal variability of the Chandler period is small (Okubo 1982), special attention is turned to the development of the damping.

4 ATMOSPHERIC AND OCEANIC EXCITATION

4.1 Consistent model configuration

In order to take geophysical excitations into account, the gyroscopic model is forced by simulated time-series of atmospheric and oceanic angular momentum. The six relevant deviation moments $\Delta \boldsymbol{I}_{ij}(t)$ of the symmetric tensor of inertia and the relative angular momentum vector $\mathbf{h}(t)$ are calculated for each time step from the global atmospheric ECHAM3-T21 general circulation model (GCM) (DKRZ 1992; Roeckner *et al.* 1992) and the global Ocean Model for Circulation and Tides (OMCT) (Thomas *et al.* 2001). Variations in the elements of the tensor of inertia are linked to atmospheric and oceanic bottom pressure variations (mass term), whereas relative angular momentum is caused by the motion of mass elements resulting from winds or oceanic currents relative to the terrestrial reference system (motion term).

The atmospheric ECHAM3 GCM is a further development for special climate studies of the weather forecast modthe European Center for Medium-Range Weather Forecast (ECMWF) at the Deutsches Klimarechenzentrum (DKRZ) in Hamburg. It uses 19 levels in the vertical (ranging from the surface to 10 hPa) with a hybrid sigma-pressure coordinate that leads to a smooth transition from the orography-following sigma coordinate in tropospheric heights to pressure levels at the top of the model atmosphere. The horizontal resolution is given by the spectral triangular truncation at wavenumber 21 (T21), corresponding to a Gaussian transform grid of approximately 5.6°.

ECHAM3 is driven by observed monthly mean sea surface temperatures and global ice coverage according to the GISST2.2 data set (Parker *et al.* 1994) for the period from 1949 to 1994. It has been shown in several studies that this forcing provides a realistic climate variability (Hense & Römer 1995; Gualdi *et al.* 1997; Hide *et al.* 1997; Glowienka-Hense 1999; Stuck 2002). The OMCT is in turn driven by twice-daily ECHAM3 forcing fields like surface pressure, wind stress, heat and freshwater fluxes. This linkage of the ocean to the atmosphere leads to consistent momentum, heat and mass fluxes at the atmosphere–ocean boundary and consequently to a thermohaline, wind- and pressure-driven oceanic circulation that is consistent with the simulated transient dynamic state in the atmosphere. In particular, there is no need for an inverse barometric (IB) correction of atmospheric pressure fields because atmospheric pressure forcing is taken into account by the ocean model. Both models yield a consistent representation of dynamics and mass redistributions in the subsystems ocean and atmosphere.

The direct effect of mass redistributions in the atmosphere and in the oceans on Earth's rotation is accompanied by loading deformations. They are calculated via Green's functions and are considered in the tensor of inertia. Gravitational influences on polar motion and variations of ΔLOD are regarded in DyMEG by adopting lunisolar torques $\mathbf{L}(t)$ and tidal deformations.

Alternative to ECHAM3 and OMCT, any other atmosphere–ocean model combination could be applied in DyMEG. From the GGFC Special Bureau for the Oceans and the Special Bureau for the Atmosphere, time-series of oceanic and atmospheric angular momentum variations can be obtained. However, it should be clearly pointed out that meaningful results can only be derived from consistent model combinations, i.e. atmosphere and ocean dynamics must match in order to include realistic compensations and to avoid artificial contributions resulting from unreal phase lags between physical processes in both subsystems.

In order to compare the ECHAM3–OMCT results with an independent atmosphere–ocean combination, the reanalysis data set of the National Centers for Environmental Prediction (NCEP) and the National Center for Atmospheric Research (NCAR) (Kalnay *et al.* 1996), which represents observed atmospheric data analysed with the analysis scheme of a weather forecast model, is adopted together with the ocean model of the MIT (Marshall *et al.* 1997; Ponte *et al.* 1998). Both time-series were also used in the spectral analysis of Gross (2000) covering the period from 1985 to 1996. As the MIT model is forced with the NCEP boundary conditions excluding atmospheric pressure variations, an inverse barometric correction has to be adopted to the atmospheric data when both models are considered. Hence, the model combinations ECHAM3–OMCT and NCEP–MIT particularly differ with respect to the pressure coupling. The NCEP data set that is applied in this study has a temporal resolution of 6 h (hereafter referred to as 6 h-NCEP). The temporal resolution of the MIT angular momentum series is 5 d.

The ECHAM3 GCM simulates realistic climate variability although no atmospheric observation enters the model. Therefore, the model combination ECHAM3–OMCT seems to be an adequate tool for studying the mechanisms of the Earth's rotational dynamics because numerical results and underlying model physics are consistent. The consideration of atmospheric pressure variations and the simultaneous computation of ocean tides and general circulation in OMCT gets this combination ahead of 6 h-NCEP–MIT from the exploratory point of view. In contrast to assimilated models, which produce residuals that are mostly not interpretable, the unconstrained model combination ECHAM3–OMCT allows a comprehensive interpretation.

On the other hand the combination 6 h-NCEP–MIT synchronizes with the realities because the reanalysis is based on observations. Consequently, phase relations of simulated and real atmospheric and oceanic oscillations are coherent. Therefore, better agreement with observed variations of Earth's rotation can be expected on the weather timescale. However, as the oceanic MIT angular momentum time-series only cover a range of 11 yr between 1985 and 1996, the numerical results of DyMEG are rather short for significant conclusions.

4.2 Atmospheric excitation

First of all the effect of the atmosphere on polar motion is analysed separately. As atmospheric mass redistributions are dominated by annual variability, the gyro is expected to reproduce the

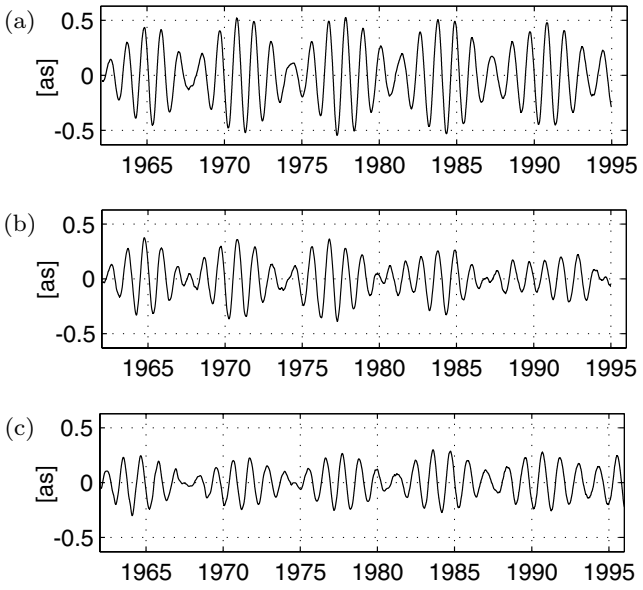

Figure 2. Resulting model time-series of the x-component of polar motion regarding atmospheric excitation of (a) ECHAM3 and (b) 6 h-NCEP in comparison with (c) geodetic observation C04. Linear trends have been removed.

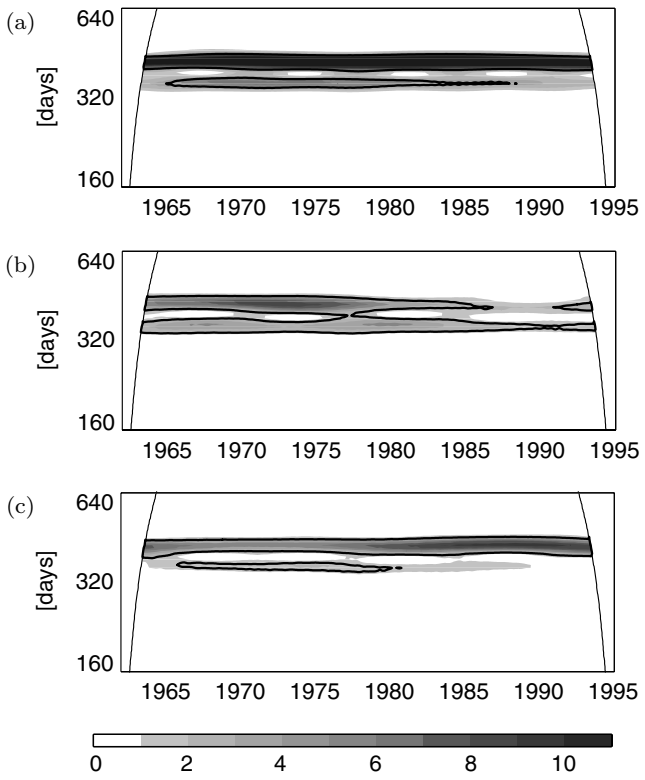

Figure 3. Morlet wavelet power spectra (normalized by variance of time-series) of atmosphere driven polar motion results (x-component) as derived from (a) ECHAM3 and (b) 6 h-NCEP; (c) geodetic observation C04. Values of variances <1 are masked out, values significant at the 1 per cent level are marked in bold outline.

typical observed polar motion characteristics, i.e. a long-term modulation resulting from the superposition of the Chandler wobble and the annual signal. Based on the findings pointed out by Gross (2000) that no significant spectral power of atmospheric excitation exists near the Chandler frequency, an undamped result for this beat would be an indicator that excitation power resulting from the stochastic weather is sufficient for the maintenance of the Chandler amplitude.

Fig. 2 compares the x-component of polar motion resulting from a ECHAM3 forced simulation with the observed polar motion series C04 for the range between 1962 and 1995. The linear trends have been removed from the time-series. As both annual and Chandler wobble are almost circular, the result for the y-component looks alike. The simulated oscillation is undamped and the observed beat is reproduced quite reasonably.

This experiment is repeated using the 6 h-NCEP reanalysis data set for the same period. As the ECHAM3 simulation does not presume inverse barometric response of the oceans to atmospheric pressure variations, a corresponding 6 h-NCEP data set without IB correction is applied. During the first 20 yr of the simulation, characteristics of the polar motion series driven by 6 h-NCEP and ECHAM3 are quite similar (*cf*. Fig. 2). However, in contrast to the latter, 6 h-NCEP produces an oscillation that features a collapsing beat after 1980.

Because contributions from atmospheric pressure variations are not compensated by corresponding sea surface variations in this atmosphere-only experiment, simulated atmospheric induced polar motion amplitudes are overestimated in comparison with the observations. The correlation coefficients between model results and observations are about 0.71 (ECHAM3) and 0.67 (6 h-NCEP). The somewhat lower correlation between 6 h-NCEP and C04 is mainly caused by weak polar motion amplitudes in the years after 1980.

A spectral analysis of both time-series by means of Morlet wavelet transformation reveals that the excitation of the Earth's free oscillation drops in the last 15 yr of the 6 h-NCEP simulation (Fig. 3b), while the Chandler amplitude is permanently excited and rather stable over the whole period of 33 yr in the ECHAM3 forced model-run (Fig. 3a).

The effects of atmospheric wind and pressure variations were inspected separately. Fig. 4 displays the results for polar motion (x-component) due to the ECHAM3 mass and motion term and the respective results of the 6 h-NCEP simulations. Obviously and not surprisingly, the predominant part of polar motion is excited by pressure variations. Since mass and motion term are not in phase, the wind term tends to counteract the pressure term. Consequently, amplitudes are reduced with respect to the mass term, when the influences of wind and pressure are superposed (*cf*. Fig. 2). This separated experiment reveals that the decreased amplitude of the combined 6 h-NCEP result after 1980 (Fig. 2b) can be fully ascribed to the pressure term, whereas the time-series produced by the motion term appears to be uniform.

The collapsing 6 h-NCEP amplitude after 1980 can possibly be attributed to artificial pressure tendencies in the NCEP reanalyses. A decrease of surface pressure was found by Hines *et al.* (2000) in the southern hemisphere around Antarctica near 65°S. Within the present investigation, a contrary tendency of the surface pressure was detected above central Asia where the comparison of mean pressure values of the intervals 1993–1997 and 1962–1966 revealed an increase of the surface pressure of up to 4 hPa (Fig. 5). As pressure variability in this region is highly linked to polar motion excitation (Nastula & Salstein 1999), the reason for the decreased amplitude of polar motion might be founded here.

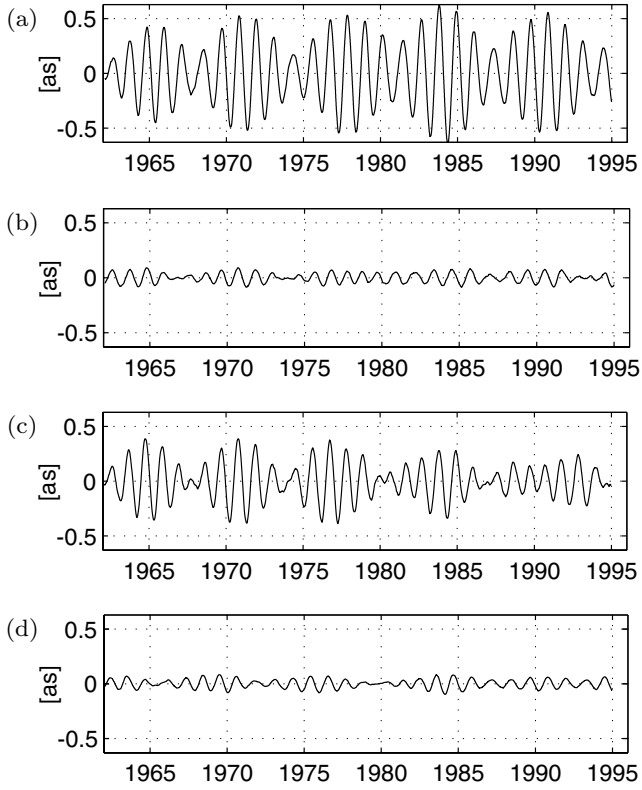

Figure 4. Resulting model time-series of the x-component of polar motion from separate model-runs for atmospheric mass and motion components: (a) ECHAM3 mass, (b) ECHAM3 motion, (c) 6 h-NCEP mass and (d) 6 h-NCEP motion. The linear trends have been removed.

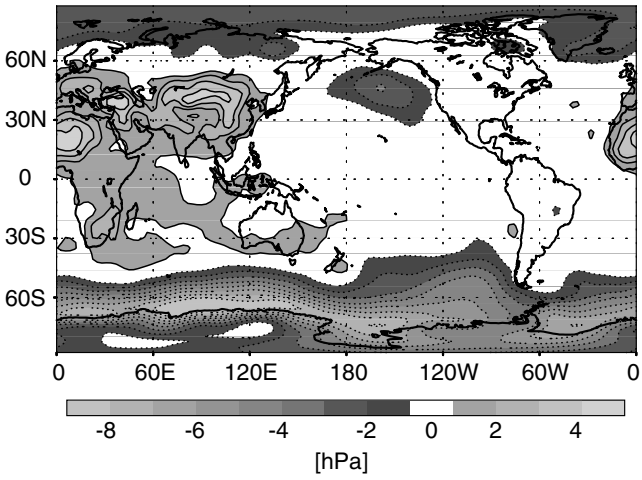

Figure 5. Difference plot of the mean NCEP surface pressure values of the intervals 1993–1997 and 1962–1966 (hPa).

4.3 Oceanic excitation

Analogously, oceanic contributions to polar motion are studied separately from the atmospheric component. To assure a quasi-steady state circulation produced by OMCT and, consequently, to avoid numerical trends caused by numerical adjustment of ocean dynamics to ECHAM3 forcing fields, the ocean-forced model-runs of DyMEG are started 1975. Because ocean pole tides are not taken into account by OMCT, this effect is considered in DyMEG by the surcharge Δk_2^O in the pole tide Love number k_2 (*cf*. Section 3).

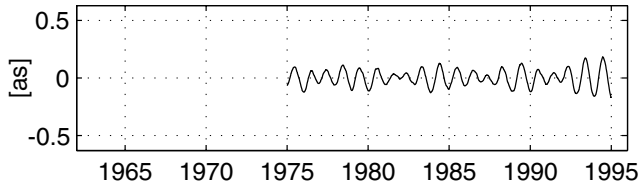

Figure 6. Resulting model time-series of the x-component of polar motion applying OMCT excitation (combined effect of mass and motion term). The linear trend has been removed.

The polar motion result derived from OMCT excitation is given in Fig. 6. Separated results for mass and motion excitation qualitatively resemble the respective ECHAM3 time-series. Again, mass variations prevail, even though the discrepancy between amplitudes of mass and motion term is less pronounced than in the atmospheric results. The oscillation simulated with the OMCT motion term shows a similar amplitude as in the respective atmospheric ECHAM3 series (Fig. 4b).

When the ocean was forced with atmospheric pressure variations, no assumption was made with respect to the reaction of the sea surface. However, annual oscillations of the mass terms of ECHAM3 and OMCT are nearly out of phase, which indicates that the simulated oceanic response is very near to that of an inverted barometer. Consequently, annual atmospheric and oceanic contributions to polar motion are expected to compensate each other partially when the excitations are superposed.

4.4 Combined atmospheric–oceanic excitation

4.4.1 Model result for ECHAM3—OMCT

The experiments with separated atmospheric and oceanic forcing indicate that both atmospheric and oceanic mass variations imply obvious contributions to polar motion excitation. Thus, coupling between the two subsystems is essential when simulating their combined influence on polar motion. As pressure coupling between ECHAM3 and OMCT is regarded, the phase relations between atmospheric and oceanic excitations are conserved. The entire effect of atmospheric and oceanic excitations resulting from both mass and motion terms of ECHAM3 and OMCT on the simulated polar motion is illustrated in Fig. 7(a).

Over the whole time range of 20 yr, the resulting polar motion is in good agreement with the observations (Fig. 7b), albeit the polar

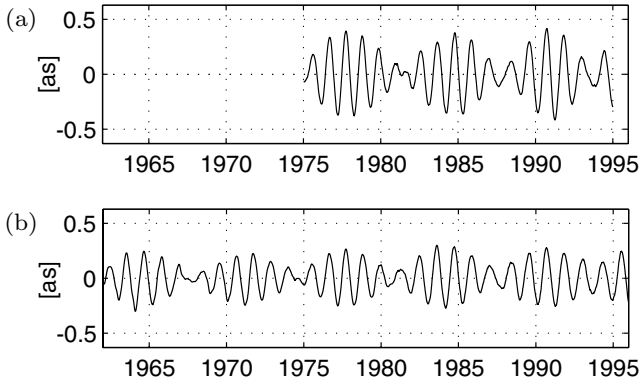

Figure 7. Model result for the x-component of polar motion applying full atmospheric and oceanic excitation. (a) Model combination ECHAM3-T21 and OMCT; (b) geodetic observation C04. The linear trends have been removed.

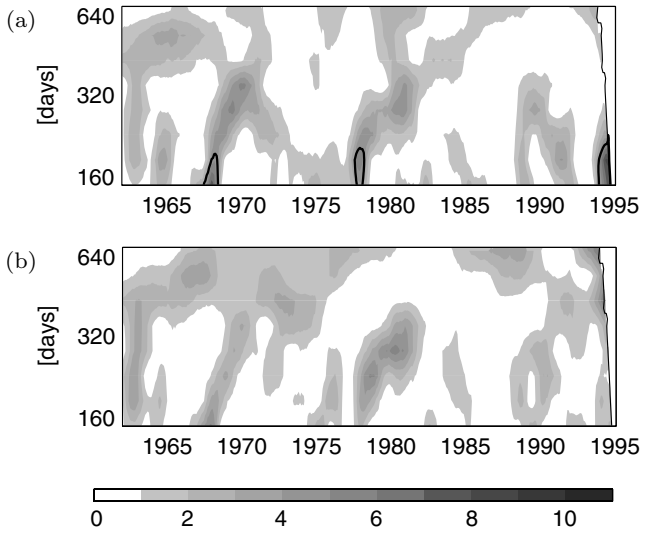

Figure 8. Morlet wavelet power spectra (normalized by variance of time-series) of atmospheric and oceanic angular momentum $\Delta \boldsymbol{I}_{13}\ \omega$. (a) ECHAM3 AAM (atmospheric angular momentum); (b) OMCT OAM (oceanic angular momentum). Annual variability is reduced. Values of variances <1 are masked out, values significant at the 1 per cent level are marked in bold outline.

motion amplitude is overestimated. The correlation coefficient between the ECHAM3–OMCT forced model result for polar motion and the geodetic observations reaches 0.95, which is a striking result as the model combination is unconstrained. As a result of the circular trait of polar motion, similar agreement with the C04-series is achieved for the y-component of the simulation. The beat due to the superposition of free and forced polar motion is undamped.

Note that no increased excitation power can be found in either spectra of ECHAM3 and OMCT in the Chandler frequency range (Fig. 8). Thus, explicit excitation near the Chandler frequency is not necessary to perpetuate the Earth's free wobble. Ongoing stochastic weather phenomena yield a random distribution of excitation power over the whole spectrum. Obviously, the excitation power of this flat distribution is strong enough to provoke a resonant reaction of the rotating Earth via rotational deformations.

In contrast to the analytical approach, the numerical solution of the Liouville equation allows the consideration of the elements $\Delta \boldsymbol{I}_{11}$, $\Delta \boldsymbol{I}_{22}$ and $\Delta \boldsymbol{I}_{12}$ of the Earth's tensor of inertia. For the model combination ECHAM3–OMCT these quantities were computed. A numerical experiment showed, that their influence on the resulting time-series is smaller than 5 mas for polar motion and 10 μs for ΔLOD. Although the effect on polar motion is larger than the accuracy of space geodetic observations, it is far below the present accuracy of modelling. Hence, the neglect of these quantities in the analytical approach seems justified.

4.4.2 Assessment of the damping

So far, the numerical value of the Love number $k_2 = 0.35 + 0.0035i$ was applied. As noted previously, this value is equivalent to a quality factor of $Q = 84$. A larger value for the imaginary part of k_2, i.e. a smaller quality factor Q, leads to a diminution of the Chandler wobble. Conversely, a smaller value for the imaginary part of k_2, which is equivalent to a larger quality factor Q, yields an amplification of the Earth's free polar motion.

Spectral analyses of the geodetically observed polar motion time-series (Gibert *et al.* 1998) show slightly increasing amplitudes of the Chandler wobble during the last decades (*cf*. Fig. 3c). Therefore, the geophysical excitations are not only expected to counteract the damping but even to produce a slight amplification of the Chandler wobble over the considered time range.

In order to assess an appropriate quality factor for the gyroscopic model, the ECHAM3–OMCT experiment is repeated several times with modified imaginary parts of the pole tide Love number within a sensitivity analysis of DyMEG Seitz & Kutterer (2004). The value of $\boldsymbol{I}mk_2$ is altered between 0 (no damping) and 0.0060 ($Q = 48$). During this experiment, the forcing conditions of DyMEG are kept unchanged. The amplitudes of the resulting time-series diverge as a result of modified damping. Phase and period of the Chandler wobble are not influenced by a change of the imaginary part of k_2.

Maximum agreement between the model result for the free polar motion and the observed Chandler amplitude is obtained for the Love number $k_2 = 0.35 + 0.0042i$, i.e. a quality factor of $Q = 68$ for the ECHAM3–OMCT forced system. Hence, this value for the pole tide Love number is appropriate for the present model setup as the excitation power that is contained in the ECHAM3 and OMCT angular momentum series is sufficient to counteract this damping and produce the slight observed amplification of the Chandler wobble. However, depending on the applied excitation series, the optimum damping factor can vary as the high-frequency atmospheric variations produced by other models might differ from those simulated by ECHAM3 (Seitz & Kutterer 2004).

4.4.3 Model results for NCEP–MIT

In order to support the conclusions drawn from the ECHAM3–OMCT result, a second atmosphere–ocean forced model-run is performed using the atmospheric 6 h-NCEP reanalyses and the global ocean circulation model of the MIT. In this investigation, the inverse barometric approximation has to be applied to the atmospheric data because the oceanic simulations did not take into account atmospheric pressure forcing. The oceanic angular momentum series of the MIT only cover 11 yr from 1985 to 1996. Therefore, the resulting polar motion time-series is rather short for reliable statistical evaluations as well as for investigations on the appropriate quality factor for this atmosphere–ocean combination.

Fig. 9(a) shows the simulated 6 h-NCEP–MIT polar motion series. Again, the beat due to Chandler and annual polar motion is visible and the correlation coefficient with the observations amounts to 0.97. However, conclusions with respect to the temporal

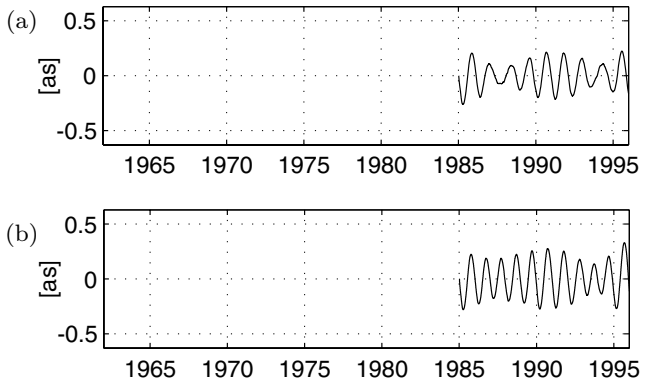

Figure 9. Model result for the x-component of polar motion applying atmospheric NCEP and oceanic MIT forcing. (a) Model combination 6 h-NCEP and MIT; (b) model combination 24 h-NCEP and MIT. The linear trends have been removed.

Table 1. Correlations between the atmospheric and oceanic forced model results for polar motion and the geodetic observations C04 (x- and y-components). Amplitudes are given in arcseconds and phases are given in degrees.

	Correlation with C04		Annual wobble x-component		Chandler wobble x-component		Annual wobble y-component		Chandler wobble y-component	
Time-series	x-comp.	y-comp.	Amplitude	Phase	Amplitude	Phase	Amplitude	Phase	Amplitude	Phase
ECHAM3–OMCT	0.95	0.94	0.17	200.53	0.21	2.74	0.17	294.08	0.21	93.53
6 h-NCEP–MIT	0.97	0.98	0.08	189.35	0.16	161.00	0.08	295.93	0.17	252.30
24 h-NCEP–MIT	0.54	0.53	0.26	189.39	0.07	108.56	0.23	283.91	0.07	202.85
C04 observation	–	–	0.09	204.42	0.16	357.81	0.08	292.97	0.16	89.54

development of the Earth's free polar motion should be handled with care since the MIT data only cover about 9 cycles of the Chandler wobble in contrast to almost 17 cycles covered by ECHAM3–OMCT. In particular, it would be interesting to see whether the Chandler wobble was perpetuated over a longer period as it was presumed by Gross (2000) or if the amplitude of polar motion collapses like in the separated 6 h-NCEP experiment (*cf*. Fig. 2b).

The result of this model-run is compared to a run which is forced by modified atmospheric data. So far the NCEP angular momentum was deduced from the highly resolving 6 h-NCEP reanalyses. In order to study the effect of high-frequency atmospheric oscillations on polar motion, the 6-hourly NCEP-forcing is exchanged by smoothed angular momentum time-series with 24 h resolution.

The polar motion series of DyMEG forced by the 24 h-NCEP and MIT angular momentum (Fig. 9b) is dominated by an annual signal with only weak interannual modulation what indicates that the Chandler amplitude is comparatively weak in contrast to C04 and the previous model-runs. The correlation coefficient between the 24h-NCEP–MIT forced simulation and C04 amounts to 0.54. This result affirms the assumption that stochastic high-frequency weather variations play an important role for polar motion excitation. To assure the reliability of this result, the model-run is repeated with modified initial values for m_i which does not lead to significant effects on the resulting time-series. When discussing the NCEP–MIT forced model results, it should be considered, that these forcing combinations do not account for the reaction of the oceans at diurnal periods due to the missing pressure coupling of the two subsystems. High-frequency atmospheric effects might be strongly accompanied by the non-barometric reaction of the oceans and the above results might be invalidated by taking into account this effect. Here, an open question remains and the result of the ECHAM3–OMCT model combination seem more trustful.

In order to compare the numerical results of DyMEG as they were derived from the three considered atmosphere–ocean combinations, Table 1 compiles the correlation coefficients between the x- and y-components of the model time-series and C04 as well as the respective phases and amplitudes of the annual and the Chandler wobble.

For ECHAM3–OMCT, the phases of both annual and Chandler wobble are in very good agreement with C04, whereas the resulting Chandler phase differs significantly from the observations in the case of NCEP–MIT. On the other hand, the amplitudes of annual and Chandler wobble are reproduced much better by 6 h-NCEP–MIT while the annual signal seems to be overestimated by the model combination ECHAM3–OMCT. Here, the reason for the increased polar motion amplitude is founded (*cf*. Fig. 7).

5 CONCLUSIONS

Variations of Earth's rotation are investigated in the time domain using the free gyroscopic model DyMEG. Period and damping of the Chandler wobble are generated by the model from realistic geometric and rheological properties of the Earth. This is in contrast to most of the previous studies where the features of the Chandler wobble are assessed from observed polar motion series because they represent a degree of freedom. The consideration of rotational deformations in the gyro lengthens the free oscillation from the Euler period to the Chandler period. It is shown that the period of the free wobble that is produced by the gyro is consistent with geodetic observations.

The Love number k_2 that is used in this study accounts for the effects of ocean pole tides and mantle anelasticity. So far, core and mantle are assumed to be fully decoupled. Without explicit excitation, the free oscillation of the gyroscopic model is a damped oscillation.

The particular interest of this study is the interaction of forced and free polar motion. As rotational deformations are a back-coupling mechanism of polar motion on the Earth's rotational dynamics, both period and amplitude of the Chandler wobble are time-dependent when additional forcing from geophysical and gravitational excitations is considered. While variations of the Chandler period are marginal, the influence of forced polar motion on the amplitude of the free wobble is obvious because damping is absent in time-series of the geodetically observed polar motion and the amplitude of the Chandler wobble even increases slightly during the last decades.

In order to study the effect of atmospheric and oceanic mass redistributions on the Chandler wobble, consistent atmospheric and oceanic angular momentum series from the model combination ECHAM3–OMCT are introduced into the gyroscopic model. The numerical results show significant agreement with geodetic observations during 1975–1994. The correlation coefficient between simulated and observed polar motion is 0.95 because the simulated beat of annual and Chandler wobble is undamped and the phases of annual and Chandler wobble are in good agreement with the C04 series.

From numerical experiments with DyMEG, the optimum quality factor for the present ECHAM3–OMCT forced model setup is found to be $Q = 68$. As the NCEP–MIT time-series is too short for comparable investigations, further insight into this topic is expected from replacing the MIT excitation series by the ECCO model simulation that is also forced by NCEP (Seitz & Kutterer 2004). ECCO is a further development of MIT and the simulations cover a range of two decades.

Oceanic mass redistributions counteract the atmospheric mass variations indicating that the ocean's response to atmospheric pressure variations is close to that of an inverted barometer. As pressure coupling is regarded in the ECHAM3–OMCT combination, high-frequency weather characteristics are transferred into the ocean. Therefore, the oceanic mass variations and consequently the oceanic excitation series are similar to the atmospheric pressure variability, however, with opposite sign. Minor contributions to polar motion are caused by the motion terms of atmospheric and oceanic angular

momentum, which in general only reduce the amplitudes of mass-generated oscillations.

As no increased excitation power is found in the range of the Chandler frequency of the ECHAM3–OMCT excitation series, it is presumed that ongoing stochastic processes in the atmosphere resulting from the weather and consequent oceanic mass redistributions account for the perpetuation of the Earth's free wobble. Stochastic excitations yield a flat distribution of excitation power over the whole spectrum, which is apparently strong enough to provoke a resonant reaction of the rotating Earth via rotational deformations. The presented numerical long-term integrations that cover the time interval between 1975 and 1994 corroborate this assumption as damping vanishes when atmospheric, oceanic and gravitational excitations are regarded in the gyroscopic model.

Gross (2000) pointed out that, in particular, oceanic bottom pressure variations were responsible for the perpetuation of the Chandler amplitude. This assumption is tested by introducing the respective atmospheric and oceanic angular momentum time-series of the model combination 6 h-NCEP–MIT and 24 h-NCEP–MIT for the period 1985–1996 into the gyroscopic model. According to the above study, the resulting Chandler oscillation that is produced by the gyro under the influence of geophysical and gravitational excitation is expected to resemble the observed one, even though no explicit information about free oscillation is predetermined in the model. However, the comparison of two model-runs applying the oceanic MIT forcing in combination with highly frequent 6 h-NCEP and smoothed 24 h-NCEP angular momentum series, respectively, reveals the importance of high-frequency atmospheric variations for polar motion excitation as the correlation coefficient between the 24 h-NCEP–MIT result and the geodetic observations amounts to only 0.54 instead of 0.97 for 6 h-NCEP–MIT.

The conclusion that the high-frequency weather is responsible for the maintenance of the Chandler amplitude is supported by the results of the experiments with separated atmospheric and oceanic excitations. Atmospheric pressure variations alone are able to maintain an undamped amplitude of polar motion (*cf* . Fig. 4). Therefore, atmospheric pressure variations were found to be the prominent hurriers of the undamped simulated polar motion.

ACKNOWLEDGMENTS

This paper was developed within the scope of a project supported by DFG grants DR 143/10 and HE 1916/4–1. The authors thank the Deutsches Klimarechenzentrum, Hamburg, Germany, for providing the ECHAM3 data set. NCEP reanalysis data was provided by the NOAA-CIRES Climate Diagnostics Center, Boulder CO, USA. Moreover, the authors are grateful to Dr. Hansjörg Kutterer (DGFI) and the referees Christian Bizouard (SYRTE) and Olivier de Viron (ROB) for their constructive remarks on the manuscript.

REFERENCES

Brzezinski, A., 2001. Diurnal and subdiurnal terms of nutation: a simple theoretical model for a nonrigid Earth, in *Proceedings of the Journées Systémes de Référence Spatio-temporels 2000*, pp. 243–251, ed. Capitaine, N., Observatoire de Paris, Paris.

Deutsches Klimarechenzentrum (DKRZ) Modellbetreuungsgruppe, 1992. *The ECHAM3 atmospheric general circulation model* Techn. Rep. No. 6, DKRZ, Hamburg.

Dziewonski, A.M. & Anderson, D.L., 1981. Preliminary Reference Earth Model (PREM), *Phys. Earth planet. Int.,* **25,** 297–356.

Furuya, M., Hamano, Y. & Naito, I., 1996. Quasi-periodic wind signal as a possible excitation of Chandler wobble, *J. geophys. Res.,* **101,** 25 537–25 546.

Furuya, M., Hamano, Y. & Naito, I., 1997. Importance of wind for the excitation of Chandler wobble as inferred from wobble domain analysis, *J. Phys. Earth,* **45,** 177–188.

Gibert, D., Holschneider M. & Le Mouël, J.-L., 1998. Wavelet analysis of the Chandler wobble, *J. geophys. Res.,* **103,** 27 069–27 089.

Glowienka-Hense, R., 1999. Forced and free Variability of the Semi-Annual Wave in the ECHAM GCM, *Climate Dynamics,* **15,** 269–275.

Gross, R.S., 1986. The influence of earthquakes on the Chandler wobble during 1977–1983, *Geophys. J. R. astr. Soc.,* **85,** 161–177.

Gross, R.S., 1992. Correspondence between theory and observations of polar motion, *Geophys. J. Int.,* **109,** 162–170.

Gross, R.S., 2000. The excitation of the Chandler Wobble, *Geophys. Res. Lett.,* **27,** 2329–2332.

Gualdi, S., Navarra, A. & von Storch, H., 1997. Tropical Intraseasonal Oscillation Appearing in Operational Analyses and in a Family of General Circulation Modells, *J. Atmos. Sci.,* **54,** 1185–1202.

Hameed, S. & Currie, R.G., 1989. Simulation of the 14-Month Chandler Wobble Climate Model, *Geophys. Res. Lett.,* **16,** 247–250.

Hense, A. & Römer, U., 1995. Statistical analysis of tropical climate anomaly simulations, *Climate Dynamics,* **11,** 178–192.

Hide, R., Dickey, J.O., Marcus, S.L., Rosen, R.D. & Salstein, D.A., 1997. Atmospheric angular momentum fluctuations during 1979–1988 simulated by global circulation models, *J. geophys. Res.,* **102,** 16 423–16 438.

Hines, K.M., Bromwich, D.H. & Marshall, G.J., 2000. Artificial surface pressure trends in the NCEP-NCAR Reanalysis over the Southern Ocean and Antarctica, *J. Climate,* **13,** 3940–3952.

Hinderer, J., Legros, H., Gire, C. & Le Mouël, J.-L., 1987. Geomagnetic secular variation, core motions and implications for the Earth's wobbles, *Phys. Earth planet. Int.,* **49,** 121–132.

International Earth Rotation Service (IERS), 2003. *IERS Annual Report 2002,* eds Dick, W.R. & Richter, B., Verlag des Bundesamts für Kartographie und Geodäsie, Frankfurt am Main.

Kalnay, E. *et al.*, 1996. The NCEP/NCAR 40-Year Reanalysis Project, *Bull. Amer. Meteor. Soc.,* **77,** 437–471.

Lambeck, K., 1980. *The Earth's Variable Rotation: Geophysical Causes and Consequences,* Cambridge University Press, Cambridge.

McCarthy, D.D., 2003. *IERS Conventions 2000,* IERS Technical Note No. 32, Verlag des Bundesamts für Kartographie und Geodäsie, Frankfurt am Main.

Marchenko, A.N. & Schwintzer, P., 2003. Estimation of the Earth's tensor of inertia from recent global gravity field solutions, *J. Geodesy,* **76,** 495–509.

Marshall, J., Adcroft, A., Hill, C., Perelman, L. & Heisey, C., 1997. A finite-volume, incompressible Navier Stokes model for studies of the ocean on parallel computers, *J. geophys. Res.,* **102,** 5753–5766.

Mathews, P.M., Herring, T.A. & Buffet, B.A., 2002. Modeling of nutation and precession: New nutation series for nonrigid Earth and insights into the Earth's interior, *J. geophys. Res.,* **107**, 10.1029/2001JB000390.

Mathews, P.M., Buffet, B.A., Herring, T.A. & Shapiro, I.I., 1991. Forced Nutations of the Earth: Influences of Inner Core Dynamics, Part 2: Numerical Results and Comparisons, *J. geophys. Res.,* **96,** 8243–8257.

Molodensky, M.S., 1961. The theory of nutation and diurnal earth tides, *Obs. Roy. Belg., Serie Geophysique,* **58,** 26–56.

Moritz, H. & Mueller, I.I., 1987. *Earth Rotation,* Ungar Publishing Company, New York.

Munk, W.H. & MacDonald, G.J.F., 1960. *The Rotation of the Earth: A Geophysical Discussion*, Cambridge University Press, Cambridge.

Nastula, J. & Salstein, D.A., 1999. Regional atmospheric angular momentum contributions to polar motion excitation, *J. geophys. Res.,* **104,** 7347–7358.

Okubo, S., 1982. Is the Chandler period variable?, *Geophys. J. R. astr. Soc.,* **71,** 629–646.

Parker, D.E., Jones, P.D., Folland, C.K. & Bevan, A., 1994. Interdecadal changes of surface temperature since the late nineteenth century, *J. geophys. Res.,* **99,** 14 373–14 399.

Ponsar, S., Dehant, V., Holme, R., Jault, D., Pais, A. & Van Hoolst, T., 2002. The Core and Fluctuations in the Earth's Rotation, in *Earth's Core:*

Dynamics, Structure, Rotation, vol. 31, pp. 251–261, eds Dehant, V. et al., AGU Geodynamics Series. AGU, Washington DC.

Ponte, R.M., Stammer, D. & Marshall, J., 1998. Oceanic signals in observed motions of the Earth's pole of rotation, *Nature,* **391,** 476–479.

Press, W.H., Flannery, B.P., Teukolsky, S.A. & Vetterling, W.T., 1987. *Numerical Recipes,* Cambridge University Press, New York.

Roeckner, E. et al., 1992. *Simulation of the present-day climate with the ECHAM model: Impact of the model physics and resolution,* Tech. Rep. No. 93, Max-Planck-Institut für Meteorologie, Hamburg.

Sasao, T., Okubo, S. & Saito, M., 1980. A simple theory on the dynamic effects of a stratified fluid core upon nutational motion of the earth, in, *Nutation and the Earth's Rotation,* IAU Symposia, vol. 78, pp. 165–183, eds Fedorov, E.P., Smith, M.L. & Bender, P.L., D. Reidel, Kiev.

Seitz, F. & Kutterer, H., 2002. Numerical Solutions for the Non-Linear Liouville Equation, in, *Vistas for Geodesy in the New Millennium,* IAG Symposia, vol. 125, pp. 463–468, eds Adam, J. & Schwarz, K.-P., Springer, Berlin.

Seitz, F. & Kutterer, H., 2004. Sensitivity Analysis of the Non-Linear Liouville Equation, *accepted for publication in the proceedings of the IUGG general assembly 2003,* IAG Symposia, Springer, Berlin.

Sidorenkov, N.S., 1992. Excitation mechanisms of Chandler polar motion, *Astr. Zh.,* **69,** 905–909.

Smith, M.L. & Dahlen, F.A., 1981. The period and *Q* of the Chandler wobble, *Geophys. J. R. astr. Soc.,* **64,** 223–281.

Souriau, A. & Cazenave, A., 1985. Re-evaluation of the seismic excitation of the Chandler wobble from recent data, *Earth planet. Sci. Lett.,* **75,** 410–416.

Stuck, J., 2002. Die simulierte axiale atmosphärische Drehimpulsbilanz des ECHAM3-T21 GCM, *PhD thesis*, Bonner Meteorologische Abhandlungen, 56, Asgard, Sankt Augustin.

Thomas, M., Sündermann, J. & Maier-Reimer, E., 2001. Consideration of ocean tides in an OGCM and impacts on subseasonal to decadal polar motion excitation, *Geophys. Res. Lett.,* **28,** 2457–2460.

Wahr, J.M., 1982. The effects of the atmosphere and the oceans on the Earth's wobble—I. Theory, *Geophys. J. R. astr. Soc.,* **70,** 349–372.

Wahr, J.M., 1983. The effects of the atmosphere and the oceans on the Earth's wobble and on the seasonal variations in the length of day—II. Results, *Geophys. J. R. astr. Soc.,* **74,** 451–487.

Wahr, J.M., 1985. Deformation Induced by Polar Motion, *J. geophys. Res.,* **90,** 9363–9368.